CHAPTER

2

Biomechanics of the Vestibular System: A Numerical Simulation

Carla F. Santos[*], *Jorge Belinha*[†], *Fernanda Gentil*[‡], *Marco Parente*[§], *and Renato M. Natal Jorge*[*]

[*]Faculty of Engineering of University of Porto (FEUP), Porto, Portugal [†]Institute of Science and Innovation in Mechanical and Industrial Engineering (INEGI), School of Engineering, Polytechnic of Porto (ISEP), Porto, Portugal [‡]School of Health - P. Porto, Porto, Portugal [§]INEGI, Institute of Mechanical Engineering and Industrial Management, Faculty of Engineering of University of Porto, FEUP, Porto, Portugal

2.1 INTRODUCTION

The vestibular system is located in the posterior portion of the inner ear. It is a key component to our sense of balance and movement. Any changes in this system can cause effects or symptoms such as dizziness, blurred vision, imbalance, and nausea, which are vertiginous syndrome indicators. Vertigo is reported as one of the most common symptoms in the world [1]. It is considered the third most frequent complaint in medicine, transmitting a sense of inadequacy and insecurity [2]. The main roles of the vestibular system, from a functional point of view, include the correction of any involuntary movement of the body mass center and balance position to avoid falls; the accurate perception of the body position in the environment and the perception of the direction and acceleration movements; and the control of eye movement to maintain a clear visual field when the individual, the environment, or both are in movement [3].

Gait and balance functions need the activation of three different sensory afferent systems, vestibular, visual, and proprioceptive, which integrate the information and lead to body and view stabilization. A healthy and active lifestyle demands a permanent stimulation of the vestibular system, which takes place during reactive adaptation, determining a head position in the space relative to the fundamental posture, as in relation to the displacement [3, 4].

The static balance maintenance is a complex process, which has a vestibular intervention. The postural control system results in the interaction between the input from the sensory system, the coordination of the central nervous system (CNS), and the motor output. In this way, the sensory system provides information about the corporal position segment in relation to other segments and the environment. These are transmitted and integrated with the CNS and sent to the motor system, which is responsible for the correct and appropriate activation of muscles for movements [5, 6].

The interaction between the different sensory systems happens as a consequence of the stimulation of the vestibular receptors by any head movement, which leads to a neural information transition to the cerebellum and the vestibular nuclei located in the brain stem [5, 6].

The vestibular system nuclei send signals primarily to the neural central structures that control eye movements and to the muscles that contribute to keeping an upright position. The projections to the former provide anatomical basis of the vestibulo-ocular reflex (VOR), which is required for clear vision, and the projections to the muscles that control our posture are necessary to keep us standing [4], maintain balance, and allow the visual control of motion events [3, 6].

Due to some vestibular disorders, characterized by dizziness symptoms triggered by some head positions (positional vertigo) or during the movement to one specific position of the cephalic segment (positioning vertigo), there

https://doi.org/10.1016/B978-0-12-816390-0.00002-9

are some authors such as Powers and Howley [7] stating that the receptors inside the vestibular system are sensitive to any movement change position. The head movements excite the hair cells placed in the sensitive structures, clarified in the next paragraphs, generating nervous impulses, which are sent to the CNS to recognize the new position.

Patients with vestibular dysfunction exhibit a measurable impairment in motor behavior controlled by the vestibular system (postural control and oculomotor and spatial orientation) and perceptual illusions, such as vertigo [4]. This and other clinical symptomatology will be detailed in the next section.

The reduced dimensions of such a system are an aspect that has to be reported, since the vestibular system controls all the balance function comprised in just 8 mm.

The global structure of the vestibular system consists of three semicircular canals (SCCs) placed orthogonally (Fig. 2.1) connected to a central chamber called the vestibule, comprising the saccule and utricle. The cochlea, which is responsible for the auditory part, is attached to the vestibular system.

The material constituents of the vestibular system include the membranous labyrinth enclosed in a bony labyrinth with the same shape. The tubular part of the membranous labyrinth within the SCCs is called the semicircular ducts (SCDs). In Fig. 2.1 the yellow part corresponds to the membranous labyrinth, and the green one is the bony labyrinth.

There are also two distinct fluids in the vestibular system: the perilymph, which is located between the labyrinths, and the endolymph, which is located inside the membranous labyrinth. This second fluid introduces the connection of the five sensory structures of this system: the cupulas of the three SCCs, shown in red in Fig. 2.1, and the two maculae located in the utricle and the saccule [4], shown in blue in Fig. 2.1.

Each canal is composed of a circular path of fluid continuity, discontinued by a swallow small pathway called the ampulla, where the hair cell sensory epithelium is placed, the cupula. The three cupulas in the SCCs, arranged in three orthogonal planes, are sensitive to angular (rotational) acceleration [8, 9]. The sensory cells exhibit constant discharge of neurotransmitters that are modified by the direction of cupula deflection. This output signal has an origin in the velocity of head rotation, which is why these cells can be named "rate sensors" in engineering terms. The signal response of the three canals during movement or standing balance is merged by the brain, leading to a vector representation of the instantaneous speed of head rotation relative to space. Since there are three canals on each inner ear orthogonal to each other, they can decompose a movement into three components. Each canal has a partner on the other side of the head. When one sensor of a canal is excited, the other correspondent is inhibited.

The vestibule is constituted by the otolithic structures, saccule and utricle; it comprises two macula portions, one in each sac, which support the otoconia. The macula is the correspondent to the cupula but with regard to linear accelerations. It is composed of a gel layer membrane covered with calcium carbonate crystals called otoconia and has substantially more mass than the cupula. The mass of the otolithic membrane causes the maculae to be sensitive to gravity and linear acceleration. Dedicated hair cells are one of the most functional structures contained in the gel layer and are the biological sensors that convert displacement due to head motion into neural firing [3].

When the head moves, the inertia of the otoconia bends the hair cells in the opposite direction. Bending all the hairs toward the kinocilium depolarizes the cell, inducing an increase in action potential frequency in the afferent nerve. Bending away from the kinocilium causes hyperpolarization and reduced action potential frequency [10].

The vestibular system's mechanical properties are essential to the understanding and interpretation of vestibular neurophysiological behavior. Due to the reduced dimensions of the SCCs, a computational numerical model appears

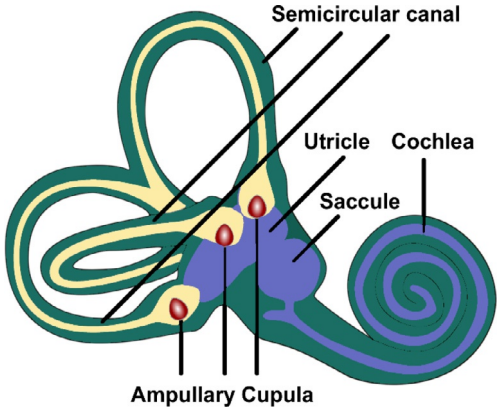

FIG. 2.1 Vestibular system with the three cupulas in each semicircular duct and both maculae in the saccule and utricle.

to be a valid research opportunity to test and validate hypotheses, such as the orientation and shape of the otolith maculae.

The patient's early evaluation also takes place in biomechanical concerns. In the last decades, research and study in the field of otoneurology of patients suffering have been developed. The outcome of such research led to quick balance recovery strategies development, preventing the onset or recurrence of vestibular disorders and consequently resulting in a fast reintegration to the daily routine.

2.2 DIAGNOSING VESTIBULAR DYSFUNCTIONS

The final goal of any health research project is to take a step into the quality improvement of the patient's daily life. A deep comprehension of the development of vestibular dysfunctions is a desirable start. In the present chapter, some of the main diseases affecting the vestibular system and respective therapies will be discussed.

The literature shows that 85% of the balance dysfunctions could be related to the inner ear disorders [11], mainly from the vestibular segment. People suffering from vertigo and dizziness have a higher risk of falls, so it is important to develop mechanisms to decrease or even eliminate these symptoms. There are high mortality and morbidity rates associated with falls in patients above 65 years old. The accidents constitute the sixth cause of death in this age group; falls are responsible for half of these episodes [12, 13]. Additionally, falls are one of the main causes of accidental bone fractures in older patients. Furthermore, the healthcare related to these kinds of fracture involves high costs, which are another strong motivation to decrease the number of people who suffer from dizziness [14].

Vertigo is one of the most common medical complaints, affecting approximately 20%–30% of the population worldwide [15]. Vertigo may be present in patients of all ages, and its prevalence increases with age, being the most frequent complaint in people over 70 years old. Additionally, vertigo is about two to three times more predominant in women than in men [16]. These numbers lead us to fathom the conditions behind the vestibular system failure. The vestibular system degeneration associated with the decrease of the CNS capacities and the aging of the human body contribute to balance changes. Other factors such as multiple and excessive medications expand the balance alterations, responsible for the vertigo occurrence and for the imbalance of the geriatric population.

The circumstances regarding the orthostatic balance correspond to the body and view stabilization, ensuring the maintenance of the gravitational center (GC) inside the sustentation polygon, either at rest or in motion [5, 17].

There are several reasons that could lead to a mismatch information between the systems in control of the balance function. When it occurs, all the system breaks, leading to equilibrium loss, until the trigger is identified and starts to compensate the central mechanisms to return balance. Consequently, vertigo can be defined as an illusionary sensation of movement. However, it is often referred to the broadest sense of dizziness, imbalance, instability, or special disorientation [5, 17].

The classification of dizziness was first performed by Drachman and Hart following [18, 19], a categorization driven by complaints of the patient, defined four categories of dizziness: presyncope (described as a feeling of imminent loss of consciousness), imbalance (or apparent sense of falling, not exclusively associated with the movement), numbness (described in Anglo-Saxon as light-headedness that does not present a clear definition or associated diagnosis), and vertigo (defined as an illusion of movement, often with sense of rotation and with nausea and vomiting). The last is the most prevalent cause of dizziness.

Vertigo can be caused by ear disorders, by the nerve connecting the ear to the brain, or even by the brain. Vertigo can also be related to visual disorders or sudden changes in blood pressure. Brain-related causes are less commonly associated with isolated vertigo and nystagmus but can still produce signs and symptoms. Many other conditions can affect the inner ear and cause vertigo, like bacterial or viral infections, cancer, abnormal pressure, nervous inflammation, or toxic substances.

Benign paroxysmal positional vertigo (BPPV) is the most common cause of vertigo, and it is described as a brief, intense sensation of spinning that occurs when there are changes in the head orientation with respect to gravity [9].

The cause of BPPV is the presence of otoconia in the SCC, which are normally located in the macula of the otolith organs, as explained in the previous section. If they fall from the utricle and become loose in the SCC, it will induce a false spinning sensation with no head rotational motion actually occurring. The sensation is generated by the distinct information sent to the brain by the two different systems, visual and vestibular [9, 20].

Therefore the BPPV diagnostic is obtained by the Dix-Hallpike maneuver, which consists of a specific set of movements performed by an audiologist, where the presence of nystagmus confirms the disorder [21].

The main effective therapy used in the reported condition is the vestibular rehabilitation composed of particle repositioning maneuvers and habituation therapy. Despite the success rates of such therapy, there are some key details that should be better analyzed. Therefore, due to the vestibular system conditions, a computational biomechanical approach seems to be a suitable analysis methodology.

2.3 NUMERICAL METHODS APPLIED TO HUMAN MORPHOLOGY

The reduced dimensions of the vestibular system hinder the experimental analysis of such a system, being the computational simulation an alternative approach to study the rehabilitation process.

In 1933, when the primary investigations of the vestibular system were performed, Steinhausen formulated a mathematical description of the SCC that considered the dynamics of the cupula endolymph system as a highly damped torsion pendulum for the sensation of the angular motion [22].

The fluid–structure interaction simulation of the endolymph and cupula during head rotation allows the measurement of the fluid interactions between the three ducts and the displacement of the cupula during the movement. This model could be useful to understand the physiological and mechanical aspects of SCC, and it could be described as a band-pass filter relating the displacement of the cupula to the angular velocity of the head [23]. Simulation methods for fluid-structure interaction include the finite element method (FEM), which have been gradually developed. FEM is a computational tool for performing mathematical analysis. It includes the use of mesh generation techniques for dividing a complex problem into small elements.

Simultaneously, meshless methods have been under strong development and are continuously extending their application field [24]. Additionally, due to the efficiency and accuracy of their discretization formulation, meshless methods are more flexible discretization techniques and a competitive and alternative numerical method in computational mechanical analysis [25].

The meshless methods discretize the domain based on a cloud of nodes [25, 26], instead of the rigid element concept used in FEM. In the early years, the solution of partial differential equations was the main focus of interest. However, today, meshless methods are applied to a wide range of applications [27].

Meshless methods can be divided into many classes or even subclasses; one of the most common classifications used is the “not-truly meshless method” or “truly meshless method” classification [27].

A meshless method is labeled “not truly” when a background mesh is required to perform the numerical integration of the integrodifferential equations ruling the studied physical phenomenon.

On the other hand, “truly” meshless methods only require an unstructured cloud of nodes to discretize the problem domain, because the influence domain, integration points, shape functions, and other necessary mathematical constructions are obtained directly from the spatial coordinates of the nodes.

Thus truly meshless methods are capable to obtain the cloud of nodes using just CAT scan or the MR images by considering the pixels (or voxels) position. Afterward, using only the nodal spatial information, these truly meshless methods are able to obtain directly the nodal connectivity, the integration points, and the shape functions. Furthermore, using a gray range of medical images, truly meshless methods are even capable of recognizing distinct biological structures and then attribute to each node the corresponding material properties [27, 28].

The natural neighbor radial point interpolation method (NNRPIM) is an example of a truly meshless method, which allows discretizing the problem domain using only a nodal cloud coming from the voxel position of the micro-CT scan (no other information is required). Then, using the natural neighbor concept, the Voronoï diagram discretizing the problem domain can be constructed. From the Voronoï diagram, it is possible to establish directly the nodal connectivity and define the position and weight of background integration points. The NNRPIM formulation and its extension to free vibration analysis were used in the present work, and some applications will be detailed in the next section.

Another popular and accurate meshless method used in this work is the radial point interpolation method (RPIM). The RPIM is an interpolator meshless method that enforces nodal connectivity using the influence-domain concept. To solve the integrodifferential equations governing the physical phenomenon, the RPIM uses a background cloud of integration points, constructed using integration cells and the Gauss-Legendre quadrature rule. This numerical integration process represents a significant percentage of the total computational cost of the analysis.

There are other meshless methods used in the present work that could be used to simulate biological structures, such as the smoothed-particle hydrodynamics (SPH), which is a computational method used also for simulating fluid flows.

It uses a Lagrangian formulation in which the particles are constant mass particles and particle mesh is attached to the material and particles deform as the material starts to deform. The SPH method works by dividing a continuous field into a set of discrete particles. These particles have a spatial distance over which their properties are "smoothed" by a *kernel function*. The particles are identified with some characteristics, such as mass, position, and velocity, but particles can also carry estimated physical properties depending on the problem, like mass density, temperature, and pressure. This method is best suited for problems in which the mesh deformations are large [29].

The SPH was first developed to simulate astrophysical fluid dynamics. Since then, it has been successfully applied to a vast range of problems, as fluid flows. It was developed by Gingold and Monaghan (1977) and Lucy (1977). A computational domain of this method is represented by computational points—particles.

This method has some advantages over grid-based techniques because its concept is simple and it is relatively easy to incorporate complicated physical effects into the SPH formalism [30, 31].

During 1995 Liu and his team [32], after some tests with SPH conditions, proposed a reproducing kernel particle method that improves the accuracy of SPH approximation.

SPH method was initially developed as a probabilistic meshless particle method and was later modified to a deterministic meshless method. Over the years the method has been optimized to increase the accuracy solution and to be applied in most of the cases.

In the next subchapter, there will be detailed numerical models and simulations performed with the meshless methods on the vestibular system of the inner ear.

2.4 BIOMECHANICAL MODEL OF THE SEMICIRCULAR DUCTS

In this section the computational model developed within the scope of this work is presented.

Regarding the computational analysis software, it was found that ABAQUS possesses enough flexibility to build and analyze such complex systems. ABAQUS is a commercial software, widely used in several computational mechanic fields, to build and simulate numerical models. Furthermore, it allows combining the FEM with the SPH meshless method. The first circular model built to study the vestibular system using the SPH method to simulate the endolymph is represented in Fig. 2.2. This model comprises the membrane of the duct discretized with shell elements (S3R) and the inside endolymph discretized with particle (PC3D) for the SPH method [33].

In the present model, the shell was defined as a rigid body because it does not present significant deformations. The fluid particle distribution is regular, and the sum of the volume of the particles is equal to the volume of the SCC with the cupula. The dimensions of the duct represented in Fig. 2.2 were obtained from a 3-D model of the complete vestibular system that can be found in the work of O.W. Henson et al. [34], which was constructed based on magnetic resonance imaging. The considered endolymph material properties were obtained from the literature, being $1.0 \times 10^{-3}\,\mathrm{kg/m^3}$ and $4.8 \times 10^{-3}\,\mathrm{Pa\,s}$, the density and viscosity of the endolymph, respectively [35]. Additionally, to

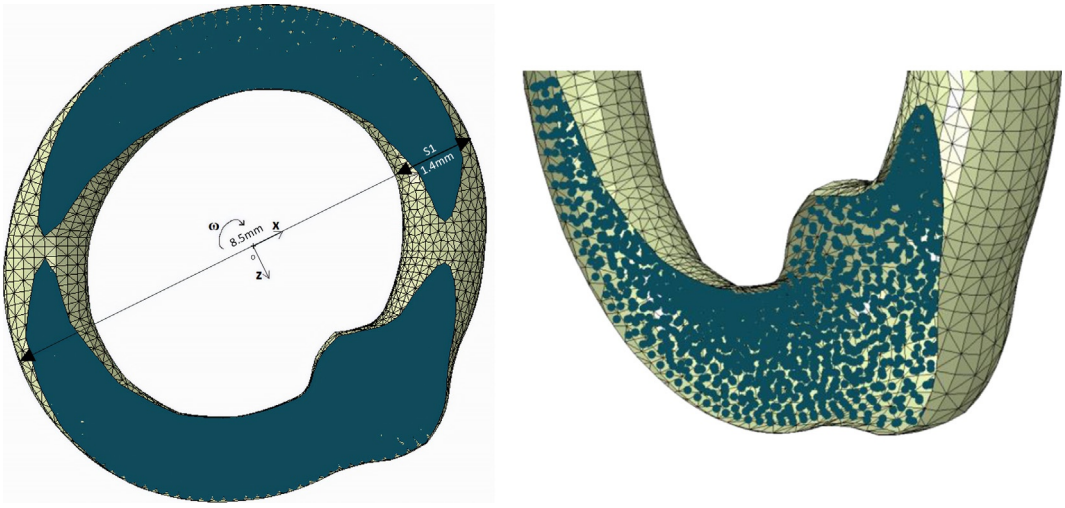

FIG. 2.2 Three-dimensional model of the semicircular duct of the vestibular system.

validate the model, three distinct particle discretization meshes were considered and analyzed, named as follows: Mesh1 (1790 particles), Mesh2 (7410 particles), and Mesh3 (13,637 particles).

Regarding the essential boundary conditions, to each node of the elements belonging to the membrane, a prescribed time-dependent angular velocity ($\omega = \pi/2\,\mathrm{rad/s}$) is enforced, with respect to point O in Fig. 2.2. To analyze the biomechanics of the SCC model, two distinct angular velocity functions were considered: profile ω1 and profile ω2 (Fig. 2.3A); both were previously used by Selva et al. [36] and WU. Cai-qin et al. [37].

Thus this model considers the gravity acceleration along the zz-axis. The general contact between the membrane elements and the fluid particles is performed explicitly by ABAQUS. To compare and validate the results of the several meshes considered (Mesh1, Mesh2, and Mesh3) with similar works of other authors [36, 37], instantaneous and local discharge variable was analyzed in Section S1 of Fig. 2.2 (Fig. 2.3B and C). The discharge is the volume rate of fluid flow transported through a given cross-sectional area.

The results obtained in this work are closed to the solution obtained by P. Selva et al. [36] and WU. Cai-qin et al. [37] when a similar angular velocity is applied to the SCC model, regardless of the considered particle mesh. Additionally, the convergence of the analysis was confirmed.

To perceive the model behavior during the imposed angular velocity, the velocity of the fluid along time was analyzed. The fluid velocity, at some instants of the simulation, is presented in Fig. 2.4A. As it is perceptible, the inner fluid velocity increases with time, as expected. After the general analysis of the global domain, a section of the duct was analyzed in details. The velocity field results correspond to Section S1 (see Fig. 2.2) obtained when profile ω1 was applied. The Fig 2.4C shows the 2-D sectional view on the left side and the velocity 3-D distribution on the right side.

The velocity maps (Fig. 2.4A and B), representing the canal fluid flow, permitted to observe the centrifugal force and the consequent higher velocity in the cupular part, due to the duct shape. The use of a three-dimensional model allowed the visualization of evidence of a 3-D velocity field in a section of the canal in some instants of the simulation. The analysis of the fluid in the section analyzed showed, as expected, that the velocity is higher in the center of the canal (Fig. 2.4C).

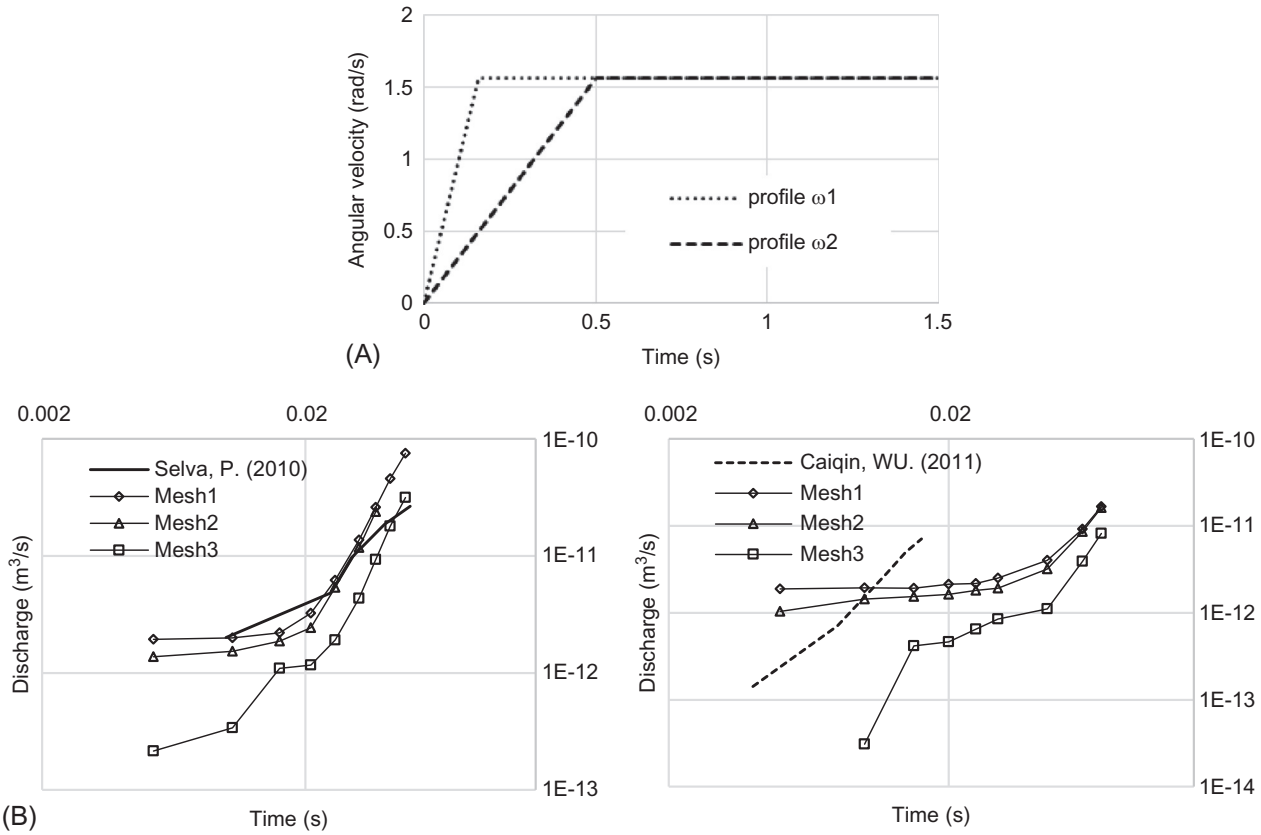

FIG. 2.3 (A) Two angular velocity functions imposed in the model, (B) discharge in the three meshes from both time steps. Profile ω1 *(left side)* and profile ω2 *(right side)*.

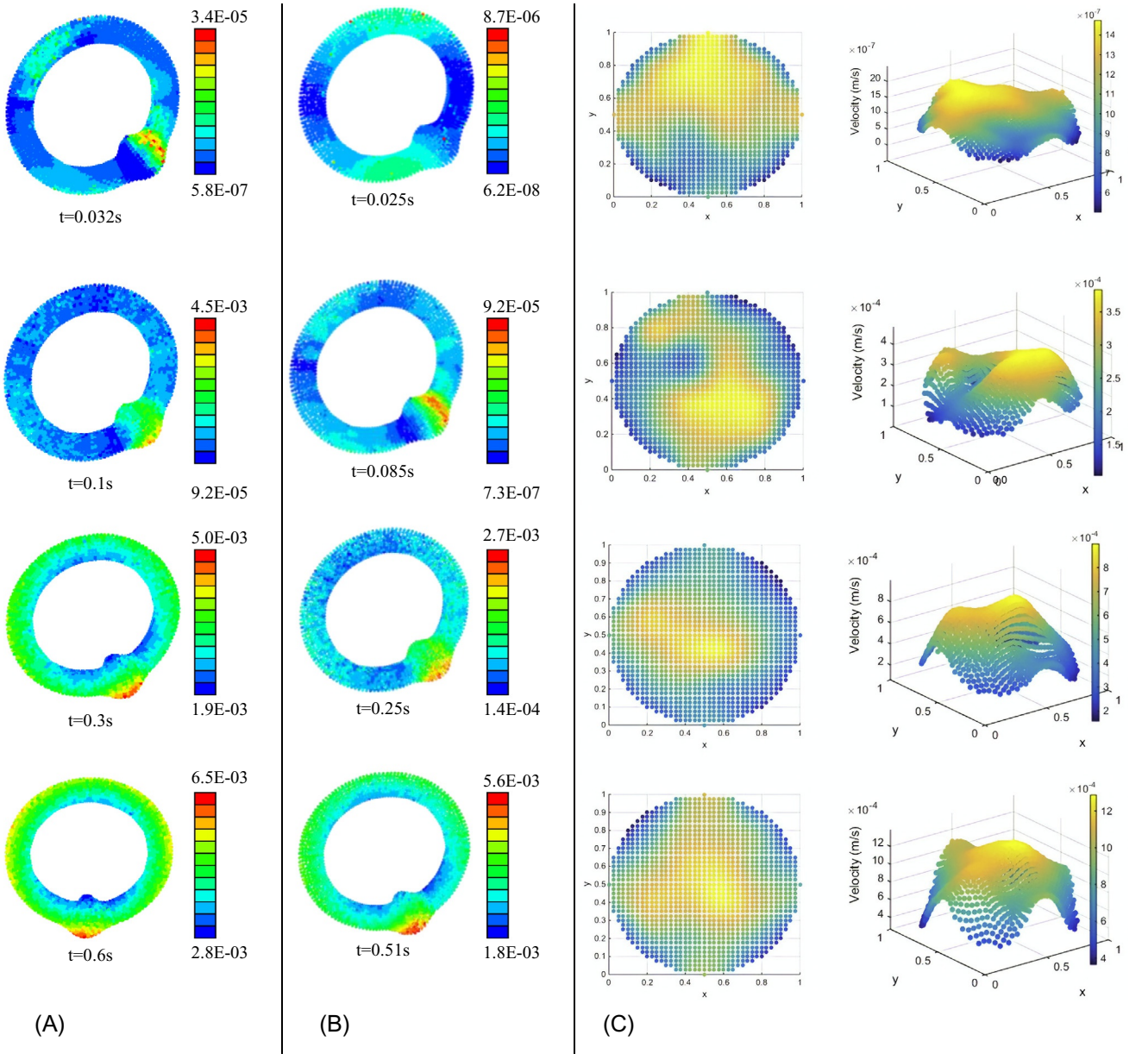

FIG. 2.4 (A) Fluid velocity (m/s) along time with profile ω1, (B) fluid velocity (m/s) along time with profile ω2, and (C) 3-D velocity field in section S1.

It was found that the use of SPH allows a more realistic representation of the fluid behavior. The applied methodology permitted to obtain promising results, according to the biomechanical properties of the vestibular system components available in the literature.

After the promising results, two more complex models of the vestibular system were built (Fig. 2.5) with the same methodology. The second model (Fig. 2.5A) was a semicircular duct with a closed shape to the real duct and with the cupula. The third model (Fig. 2.5B) was the organic vestibular system with three SCCs, a vestibule, and cupulas.

The results obtained with both models were similar to the first model, allowing us to perform new inner ear disorder simulations mainly due to the new structures.

One particular case of BPPV is cupulolithiasis, which occurs when the otoconia get lost in the SCC and attach to the cupula, inducing a false sensation of movement and leading to vertigo [38]. In the present chapter, generalized displacements of the cupula (free vibrations) will be applied to the obtained modal. The main goal was to understand the mechanical implications of the attached otoconia to the cupula.

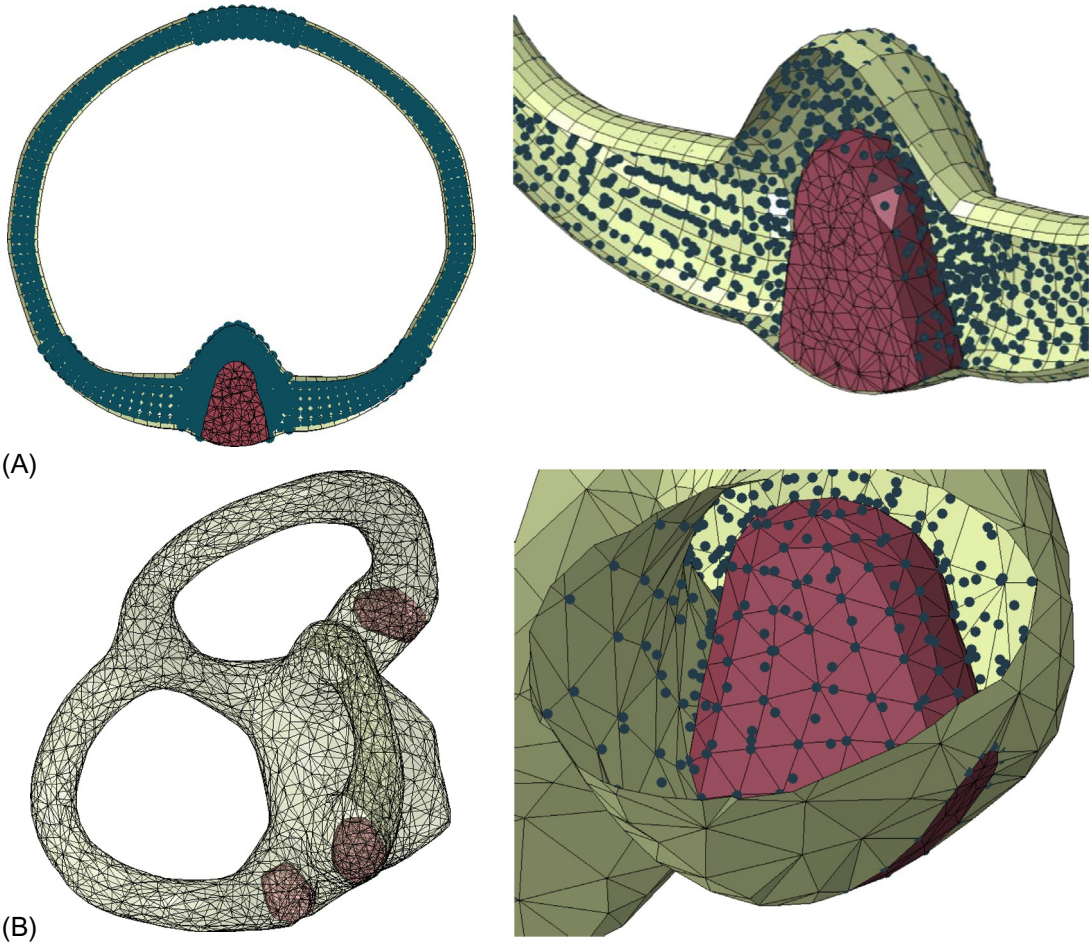

FIG. 2.5 (A) Three-dimensional model of the semicircular duct with a cupula and (B) three-dimensional model of the vestibular system.

To obtain numerically the free vibration modes of the cupula, 2-D and 3-D discrete models were built using the standard dimensions and the approximated mechanical properties found in the literature [39]; the applied boundary conditions were correlated with a real situation. Three different scenarios were simulated: the cupula itself, the cupula with the surrounded fluid, and the cupula with the attached otoconia and the surrounded fluid.

The free vibrations of the cupula were obtained with the software FEMAS, which is a finite element and meshless analysis software fully developed in an academic environment [27], and it possesses a graphical user interface (GUI) running in a MATLAB environment.

The formulations used to study the discrete models of the cupula were the FEM and two distinct meshless methods detailed in the previous section: RPIM and NNRPIM.

The results presented in this chapter include the vibration modes (Fig. 2.6) and the corresponding frequencies (Table 2.1) of the cupula 2-D with 417 nodes and 382 elements.

To visualize automatically the vibration mode, the results of the figures correspond to a fictitious displacement field. With this visualization technique, it is possible to visualize in each figure the magnitude of the fictitious displacement corresponding to the indicated vibration mode, since the red color corresponds to the higher displacement values and the blue color to the lower ones. In Table 2.1 the corresponding 10 first vibration frequencies of the cupula are presented.

The results indicate that the first vibration frequency is between 51.48 and 54.70 Hz. Note that the following vibration frequencies are much higher, which allows identifying with enough precision the magnitude of frequency of the first mode.

All the vibration frequencies obtained are contained in the human hearing range, since it goes from 20 to 20,000 Hz. In general, the vibration frequencies obtained with both meshless methods used (RPIM and NNRPIM) are lower than the ones obtained with FEM.

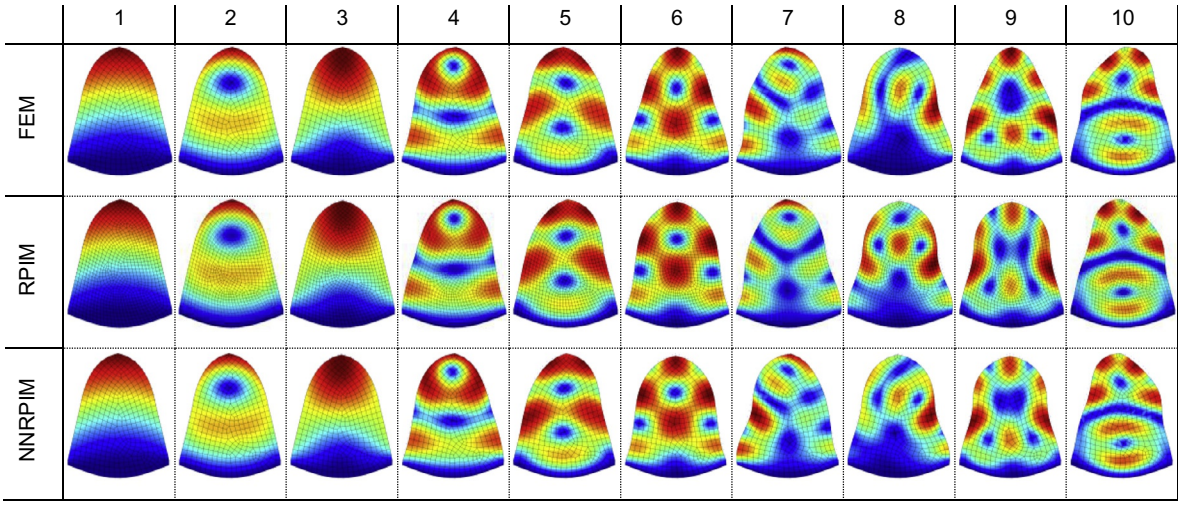

FIG. 2.6 Ten first modes of vibration of the two-dimensional cupula with FEM, RPIM, and NNRPIM.

TABLE 2.1 The 10 First Vibration Frequencies of the Two-Dimensional Cupula with FEM, RPIM, and NNRPIM

	Natural frequency (Hz)									
	1	**2**	**3**	**4**	**5**	**6**	**7**	**8**	**9**	**10**
FEM	54.70	121.32	131.62	226.17	259.80	265.13	345.26	350.33	362.51	386.60
RPIM	51.78	117.27	126.98	216.15	249.26	251.89	324.66	329.32	340.28	359.79
NNRPIM	51.48	117.36	126.35	213.64	249.12	251.08	321.02	330.41	338.08	361.29

Thus, to observe the effect of the endolymph around the cupula, the first five vibration modes of the cupula are presented in Fig. 2.7, for the FEM and both meshless methods. Note that the first two vibration modes obtained with the FEM resemble the first vibration mode obtained in Fig. 2.6. Furthermore, the third, fourth, and fifth vibration modes obtained now are very similar to the second vibration mode obtained in the analysis of the cupula without surrounding fluid.

The same effect is verified for the RPIM and NNPRIM approaches, the first vibration mode of the present RPIM analysis resembles the first vibration mode obtained in the cupula without fluid, and the second and third vibration modes of the present analysis are very similar to the second vibration mode obtained in Fig. 2.6.

Regarding the natural frequencies of the cupula surrounded by endolymph, in this study, the results obtained were 59 and 75 Hz in FEM, 61 Hz in the RPIM analysis, and 60 and 63 Hz in NNRPIM analysis, for the first resembling mode. Note that these values are closed to the ones observed in Table 2.1, indicating that the fluid has a reduced influence on the magnitude of the cupula's natural frequency.

In the next step of the present study, another possible cause of vertigo was simulated, the cupulolithiasis, which happens when the otoconia get attached to the cupula. Then, two different situations were simulated, one with one otoconium and another with three otoconia, as could be observed in the first line of Fig. 2.8.

The goal is to understand if the inclusion of the otoconia changes significantly the natural frequency of the cupula. Since the results obtained in the previous analyses with the three formulations were very similar, in Fig. 2.8, only the results regarding the NNRPIM formulation are presented.

When one otoconium (or one otoconium group) is considered, the frequencies of the cupula resembling its natural frequency (observed in Fig. 2.8) using the NNPRIM formulation are 61.42 Hz, which is also a very close result with the three-otoconium situation, which obtained 61.80 Hz for the same conditions. This may indicate that the size of the otoconium particles is not enough to change significantly the vibration frequency of the cupula [40].

The global results showed that the three different methodologies applied are capable to achieve similar results. However, most importantly, this work opens a new research branch in the computational analysis of the vestibular system.

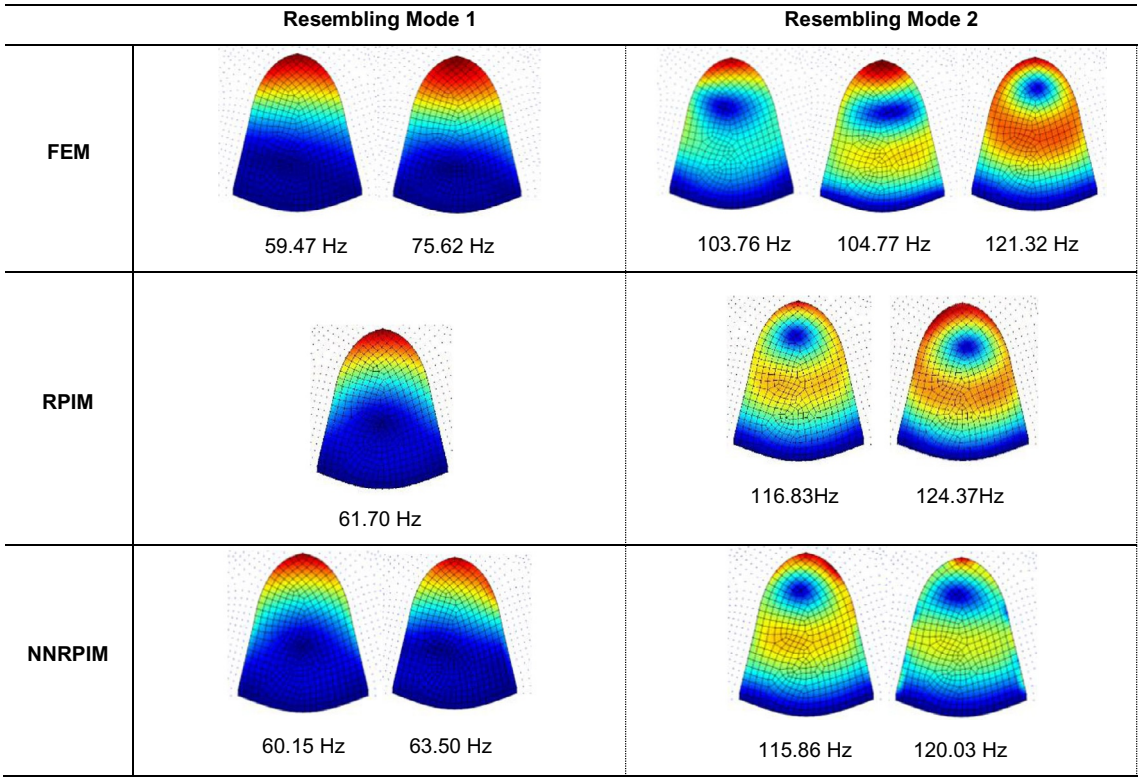

FIG. 2.7 Two first modes and natural frequencies of the two-dimensional cupula with endolymph using FEM and RPIM and NNRPIM.

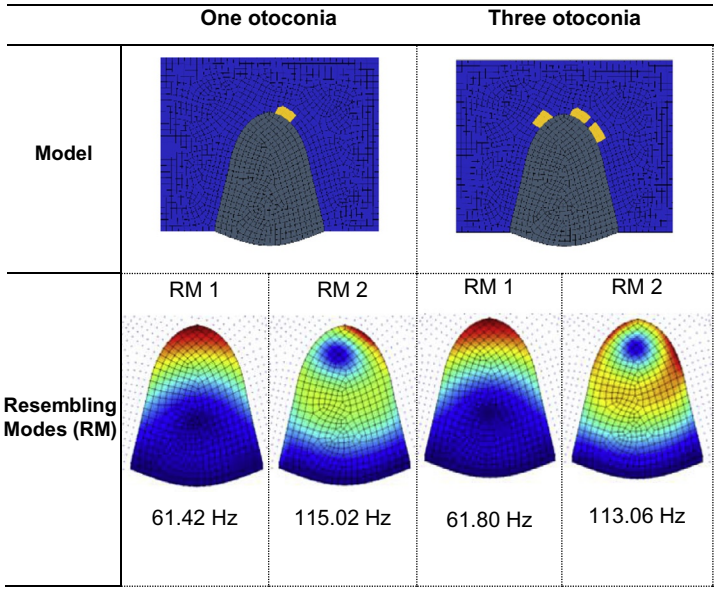

FIG. 2.8 Two first modes and natural frequencies of the cupula with endolymph and otoconia.

In conclusion, it was possible to understand that the natural frequency of the cupula ranges between 51 and 61 Hz for all the analyzed situations. Moreover, all the other vibration frequencies possess very distinct values. Since theoretically the resonance phenomena will force the cupula to vibrate, the induced vibration will allow detaching the otoconium particles from the cupula, reducing the vertigo symptoms. This could be achieved with noninvasive ways, such as listening to music with a predominant set of bass sounds.

2.5 CONCLUSIONS

The vestibular system plays an important role in the maintenance of the body balance. It is imperative to study this system considering that vertigo affects a huge part of the older population. The research work presented in this chapter has demonstrated once again the value of computational numerical simulation to study biological structures and phenomena.

In conclusion, a better comprehension of the biomechanics of the vestibular system is the first step to plan different kinds of simulations with numerical models. The vestibular system model built using several numerical methods, as FEM and meshless methods, aims to be the first step to reinvent the rehabilitation process. The development of a tool, which can help the audiologist in their daily practice, is an important step in such scientific field that can contribute to a fast recovery from vestibular disorders.

Acknowledgments

The authors acknowledge the funding by Ministério da Ciência, Tecnologia e Ensino Superior, Fundação para a Ciência e a Tecnologia, Portugal, and Programa Operacional Capital Humano (POCH), comparticipado pelo Fundo Social Europeu e por fundos nacionais do MCTES under research grants SFRH/BD/108292/2015, IF/00159/2014, and by project funding MITEXPL/ISF/0084/2017 and UID/EMS/50022/2013 (funding provided by the interinstitutional projects from LAETA). Additionally, the authors gratefully acknowledge the funding of Project NORTE-01-0145-FEDER-000022, SciTech, Science and Technology for Competitive and Sustainable Industries, co-financed by Programa Operacional Regional do Norte (NORTE2020), through Fundo Europeu de Desenvolvimento Regional (FEDER).

References

[1] H. Neuhauser, T. Lempert, Vertigo: epidemiologic aspects, Semin. Neurol. 29 (5) (Nov. 2009) 473–481.
[2] R. Humphriss, Clinical outcomes of vestibular rehabilitation, Physiotherapy 87 (7) (2001) 368–373.
[3] J.E. Hall, Guyton and Hall Textbook of Medical Physiology, 13th ed., Elsevier Inc, 2015.
[4] S.J. Herdman, Vestibular rehabilitation, Curr. Opin. Neurol. 26 (1) (Mar. 2013) 96–101.
[5] D.A. Winter, Human balance and posture control during standing and walking, Gait Posture 3 (4) (Dec. 1995) 193–214.
[6] H.C. Diener, J. Dichgans, On the role of vestibular, visual and somatosensory information for dynamic postural control in humans, Prog. Brain Res. 76 (1988) 253–262.
[7] S.K. Powers, E.T. Howley, Exercise Physiology: Theory and Application to Fitness and Performance, McGraw-Hill Humanities/Social Sciences/Languages, 2012.
[8] S. Herdman, Vestibular Rehabilitation, F.A. Davis Co., 2007.
[9] H. Reisine, J.I. Simpson, V. Henn, A geometric analysis of semicircular canals and induced activity in their peripheral afferents in the rhesus monkey, Ann. N. Y. Acad. Sci. 545 (1988) 10–20.
[10] R. Jaeger, A. Takagi, T. Haslwanter, Modeling the relation between head orientations and otolith responses in humans, Hear. Res. 173 (1–2) (Nov. 2002) 29–42.
[11] M.J. Gámiz, J.A. Lopez-Escamez, Health-related quality of life in patients over sixty years old with benign paroxysmal positional Vertigo, Gerontology 50 (2) (Feb. 2004) 82–86.
[12] P.B. Salzman, Gait and balance disorders in older adults, Am. Fam. Physician 82 (1) (2010) 61–68.
[13] U. Olsson Möller, P. Midlöv, J. Kristensson, C. Ekdahl, J. Berglund, U. Jakobsson, Prevalence and predictors of falls and dizziness in people younger and older than 80 years of age—a longitudinal cohort study, Arch. Gerontol. Geriatr. 56 (1) (Jan. 2013) 160–168.
[14] R.E. Gans, Overview of BPPV: Treatment Methodologies – Hearing Review, [Online]. Available: http://www.hearingreview.com/2000/09/overview-of-bppv-treatment-methodologies/, 2000. Accessed 16 April 2018.
[15] M. von Brevern, H. Neuhauser, Epidemiological evidence for a link between vertigo and migraine, J. Vestib. Res. 21 (6) (2011) 299–304.
[16] H.K. Neuhauser, T. Lempert, Vertigo: epidemiologic aspects, Semin. Neurol. 29 (5) (2009) 473–481.
[17] F.B. Horak, Clinical assessment of balance disorders, Gait Posture 6 (1) (Aug. 1997) 76–84.
[18] K. Hanley, T. O'Dowd, N. Considine, A systematic review of vertigo in primary care, Br. J. Gen. Pract. 51 (469) (Aug. 2001) 666–671.
[19] R.W. Baloh, Vertigo, Lancet 352 (9143) (Dec. 1998) 1841–1846.
[20] T.D. Fife, et al., Practice parameter: therapies for benign paroxysmal positional vertigo (an evidence-based review): [RETIRED], Neurology 70 (22) (May 2008) 2067–2074.
[21] A. Katsarkas, Benign paroxysmal positional vertigo (BPPV): idiopathic versus post-traumatic, Acta Otolaryngol. 119 (7) (1999) 745–749.
[22] M. Kassemi, D. Deserranno, J.G. Oas, Fluid–structural interactions in the inner ear, Comput. Struct. 83 (2–3) (Jan. 2005) 181–189.
[23] C. Wu, C. Hua, L. Yang, P. Dai, T. Zhang, K. Wang, Dynamic analysis of fluid-structure interaction of endolymph and cupula in the lateral semicircular canal of inner ear, J. Hydrodyn. Ser. B 23 (6) (Dec. 2011) 777–783.
[24] P.K.T. Belytschko, Y. Krongauz, D. Organ, M. Fleming, Meshless methods: an overview and recent developments, Comput. Methods Appl. Mech. Eng. 139 (1–4) (Dec. 1996) 3–47.
[25] G. Chen, et al., A new approach for assigning bone material properties from CT images into finite element models, J. Biomech. 43 (5) (Mar. 2010) 1011–1015.
[26] T.Q.B.T.-V. Vu, N.-H. Nguyen, A. Khosravifard, M.R. Hematiyan, S. Tanaka, A simple FSDT-based meshfree method for analysis of functionally graded plates, Eng. Anal. Bound. Elem. 79 (Jun. 2017) 1–12.

[27] J. Belinha, Meshless Methods in Biomechanics – Bone Tissue Remodelling Analysis, Lecture Notes in Computational Vision and Biomechanics, vol. 16, Springer Netherlands, 2014.
[28] T.Q. Bui, M.N. Nguyen, C. Zhang, An efficient meshfree method for vibration analysis of laminated composite plates, Comput. Mech. 48 (2) (Aug. 2011) 175–193.
[29] G.R. Liu, M.B. Liu, Smoothed Particle Hydrodynamics, World Scientific, 2003.
[30] L. Lobovský, J. Křen, Smoothed particle hydrodynamics modelling of fluids and solids, Appl. Comput. Mech. 1 (2007) 521–530.
[31] J.J. Monaghan, Smoothed particle hydrodynamics, Reports Prog. Phys. 68 (8) (Aug. 2005) 1703–1759.
[32] W.K. Liu, S. Jun, S. Li, J. Adee, T. Belytschko, Reproducing kernel particle methods for structural dynamics, Int. J. Numer. Methods Eng. 38 (10) (May 1995) 1655–1679.
[33] C.F. Santos, J. Belinha, F. Gentil, M. Parente, R.N. Jorge, An alternative 3D numerical method to study the biomechanical behaviour of the human inner ear semicircular canal, Acta Bioeng. Biomech. 19 (1) (2017) 3–15.
[34] O.W. Henson, et al., Department of Cell and Developmental Biology, University of North Carolina, Chapel Hill and The Center for In Vivo Microscopy, Duke University, Durham, NC, Copyright, 2000.
[35] J.L. Davis, J. Xue, E.H. Peterson, J.W. Grant, Layer thickness and curvature effects on otoconial membrane deformation in the utricle of the red-ear slider turtle: static and modal analysis, J. Vestib. Res. 17 (4) (Jan. 2007) 145–162.
[36] P. Selva, J. Morlier, Y. Gourinat, Development of a dynamic virtual reality model of the inner ear sensory system as a learning and demonstrating tool, Model. Simul. Eng. 2009 (2009) 1–10.
[37] C. Wu, K. Wang, L. Yang, P. Dai, Three-dimensional models of the membranous vestibular labyrinth in the guinea pig inner ear, in: Proc. 2011 4th Int. Conf. Biomed. Eng. Informatics, BMEI 2011, vol. 1, 2011, pp. 541–544.
[38] T.M. Squires, M.S. Weidman, T.C. Hain, H.a. Stone, A mathematical model for top-shelf vertigo: the role of sedimenting otoconia in BPPV, J. Biomech. 37 (8) (Aug. 2004) 1137–1146.
[39] J.L. Davis, J. Xue, E.H. Peterson, J.W. Grant, Layer thickness and curvature effects on otoconial membrane deformation in the utricle of the red-ear slider turtle: static and modal analysis, J. Vestib. Res. 17 (4) (2007) 145–162.
[40] C.F. Santos, J. Belinha, F. Gentil, M. Parente, R.N. Jorge, The free vibrations analysis of the cupula in the inner ear using a natural neighbor meshless method, Eng. Anal. Bound. Elem. 92 (Jul. 2018) 50–63.